Chemical Engineering Journal 166 (2011) 772–778

Contents lists available at ScienceDirect

Chemical Engineering Journal

journal homepage: www.elsevier.com/locate/cej

Mechanical and thermal properties of poly(lactic acid) composites with rice straw fiber modified by poly(butyl acrylate)

Lijun Qin[a], Jianhui Qiu[a,b,*], Mingzhu Liu[a,**], Shenglong Ding[a], Liang Shao[a], Shaoyu Lü[a], Guohong Zhang[b], Yang Zhao[b], Xie Fu[b]

[a] Department of Chemistry and State Key Laboratory of Applied Organic Chemistry, Lanzhou University, Lanzhou 730000, PR China
[b] Department of Machine Intelligence and Systems Engineering, Faculty of Systems Engineering, Akita Prefectural University, Akita 015-0055, Japan

ARTICLE INFO

Article history:
Received 6 July 2010
Received in revised form 20 October 2010
Accepted 9 November 2010

Keywords:
Composites
Poly(lactic acid)
Rice straw fiber
Suspension polymerization
Butyl acrylate

ABSTRACT

The rice straw fiber (RSF) was modified by suspension polymerization of butyl acrylate (BA) monomer. The results of Fourier transform infrared (FTIR) spectroscopy and scanning electron microscopy (SEM) indicated that poly(butyl acrylate) (PBA) was adsorbed and coated on RSF. The biodegradable composites were prepared with the modified rice straw fiber (MRSF) and poly(lactic acid) (PLA) by HAAKE rheometer. Mechanical properties showed that the tensile strength of PLA/MRSF composites (W(%) = 7.98) increased by 6 MPa compared with blank sample. The water absorption of the PLA/MRSF composites was lower than PLA/RSF composites. The thermal properties of these composites were investigated by thermogravimetric analysis (TGA) and differential scanning calorimetry (DSC). The TGA results confirmed that thermal stability of PLA/RSF composites increased with the PBA increasing. The DSC data showed that RSF played a role as a nucleating agent and PBA made crystallization of PLA more difficult and incomplete.

1. Introduction

Humanity is facing increasingly difficult challenges in life despite the great advancements in science and technology over the last century. All the needs of modern society, e.g., food, fuel, energy, and materials, are highly dependent on diminishing fossil resources [1]. Rising oil prices and increased environmental awareness have contributed to the advance of research on and development of biocomposites [2]. Biocomposites composed of biodegradable polymer and biofiber (natural fiber) as matrix material and reinforcing element, respectively, have been attracted attention from the viewpoint of protection of the natural environment in recent years [3–5]. Biocomposites show excellent performances such as high strength and stiffness, great versatility, and processing advantages at favourable cost, which make them be extensively used in many applications, ranging from aerospace technology to the automobile industry [6].

Biodegradable polymers as matrix material of biocomposites can reduce the reliance on fossil fuels [7]. The usual biodegradable polymers include poly(butylene succinate) (PBS), poly(caprolacton) (PCL), poly(hydroxyalkanoates) (PHA), and poly(lactic acid) (PLA), and so on [8,9]. Poly(lactic acid) (PLA) is a degradable thermoplastic polymer with excellent mechanical properties and produced on a large scale from fermentation of corn starch to lactic acid and subsequent chemical polymerization. Pure PLA can be degraded into carbon dioxide, water, and methane with long-term using, compared to other petroleum plastics [10,11]. Moreover, PLA is applied widely [12]. It can be used in either the industrial packaging field or the biocompatible/bioabsorbable medical device market. It can be easily processed into molded parts, film, or fiber, and so on [1,13]. However, the high price and brittleness of PLA currently limit its application and considerable efforts have been made to improve these characteristics of the polymer [14–16].

The nature fiber comes from stalks, leaves, and seeds, such as jute, kenaf, hemp, sisal, flax, wheat straw and rice straw. [17,18]. Compared to synthetic fiber, natural fiber has many advantages such as recoverability, biodegradation, flammability, non-toxicity, and other excellent properties [19,20]. As the plant resources, rice is widely cultivated in China. The gross amount of rice straw reached 0.16 billion ton each year. Rice straw is not only a potential source of energy but also a value-added by-product [21]. At present, rice straw is poorly utilized, about 45–60% incinerated and discarded, which not only waste organic fertilizer source, but also pollute the environment. Therefore, the use of rice straw is significant to either environmental protection or cost of material [22]. Among the many types of natural fillers, rice straw fiber (RSF) has not attracted much

* Corresponding author at: Department of Machine Intelligence and Systems Engineering, Faculty of Systems Engineering, Akita Prefectural University, Akita 015-0055, Japan. Tel.: +81 184 27 2134; fax: +81 184 27 2188.
** Corresponding author. Tel.: +86 931 8912387; fax: +86 931 8912582.
E-mail addresses: qiu@akita-pu.ac.jp (J. Qiu), mzliu@lzu.edu.cn (M. Liu).

1385-8947/$ – see front matter © 2010 Elsevier B.V. All rights reserved.
doi:10.1016/j.cej.2010.11.039

attention because of low content of cellulose (28–48%) [23–25]. It was reported that the physico-chemical properties of RSF could be modulated by various derivatization techniques. RSF can be used as filler material in the PLA matrix property enhancement and to reduce costs. However, only a few numbers of studies have been so far reported for biodegradable PLA composites based on RSF due to the weak interaction between hydrophilic RSF and hydrophobic PLA [20,23].

In this investigation, composites consisting of PLA and modified rice straw fiber (MRSF) with poly(butyl acrylate) (PBA) were prepared to achieve improved mechanical and thermal properties. PBA should be more compatible than rice straw with PLA because of the interaction of the ester groups of the both, the PLA matrix and PBA [26]. PBA was chosen here to modify compatibly properties of the hydrophilic RSF and hydrophobic PLA because it is a hydrophobic polymer which adsorbed and coated on RSF. To evaluate the modified effect of PBA, the mechanical and thermal properties were characterized by tensile test, water absorption test, DSC, and TGA.

2. Experimental

2.1. Materials

Poly(lactic acid) (PLA A306 injection grade) in pellet form was obtained from Biopla Products Factory (Ningbo, China). It has a specific gravity of 1.2 and a melt flow index around 10–13 g/10 min (190 °C/2.16 kg). Its glass transition temperature (T_g) and melting temperature (T_m) are 55–60 °C and 150–155 °C, respectively. It was dried in a vacuum oven at 80 °C for 6 h before preparation of composites. Rice straw fiber (100–300 μm) obtained from commercial sources, were dried in a vacuum oven at 100 °C for 6 h to remove moisture before used. Azobisisobutyronitrile (AIBN) (China) was used as the initiator for suspension polymerization reactions. Butyl acrylate (BA) (Tianjing Chem. Reagent Co., China) was purified of inhibitor upon distillation under reduced pressure and kept refrigerated until used. Polyvinyl alcohol (PVA) (1750 ± 50) was purchased from Shanghai Reagent Co. (China). Distilled water was applied for all the polymerization and treatment processes.

2.2. Preparation of MRSF

Dried RSF and BA monomer were well-mixed in a three necked round bottom flask under ultrasonic at temperature of 20 °C, for 30 min. And then, a certain quantity of initiator, dispersant, and distilled water was added. The system was under nitrogen atmosphere and equipped with a water bath, mechanical stirrer, reflux condenser and thermometer. The weight ratio to RSF and BA monomer was 100:15, 100:20, 100:25, 100:30, 100:40, 100:50, 100:80, 100:100, 100:120 and 100:150, respectively, RSF: distilled water was 1:20 and BA monomer:AIBN:PVA was 100:3:2. The nitrogen atmosphere and agitation were maintained throughout the experiment. After reaction for 6 h at 75 °C, MRSF was obtained by leaching the reaction solution with the buchner funnel and was washed with distilled water several times. And then, the washed MFSF was dried in an oven at 80 °C for 8 h to remove moisture and then was further dried in a vacuum oven at 100 °C for 4 h to remove residual moisture.

The percentage of weight of PBA reacted on RSF, W(%), and yield of homopolymerization of PBA on RSF, Y(%), are calculated from Eqs. (1) and (2), respectively:

$$W(\%) = \frac{M_{MRSF} - M_{RSF}}{M_{RSF}} \times 100 \quad (1)$$

$$Y(\%) = \frac{M_{MRSF} - M_{RSF}}{M_{BA}} \times 100 \quad (2)$$

Table 1
Individual batch composition.

Samples	PLA (g)	MRSF			
		RSF (g)	RSF:BA (g/g)	W(%)	Y(%)
S-1	45	5	100:0	0	0
S-2	45	5	100:15	4.280	26.00
S-3	45	5	100:20	7.980	33.28
S-4	45	5	100:25	16.48	54.98
S-5	45	5	100:30	23.10	64.27
S-6	45	5	100:40	35.65	74.35
S-7	45	5	100:50	47.45	79.17
S-8	45	5	100:80	87.99	91.76
S-9	45	5	100:100	112.5	93.87
S-10	45	5	100:120	132.9	92.43
S-11	45	5	100:150	172.7	96.08

where M_{RSF} is the original weight of RSF, M_{MRSF} is the weight of the RSF after modification, and M_{BA} is the weight of BA monomer.

2.3. Preparation of composites

The PLA and MRSF were weighted at the desired addition level (Table 1) and premixed in a glass beaker. The mixture was then melt-compounded in an HAAKE rheometer (HAAKE Rhemix 600 P German) at 175 °C for 5 min at a mixing speed of 80 rpm/min. The melted compounds were hot-press molded at 175 °C.

2.4. Characterization

2.4.1. Fourier transform infrared spectroscopy

Fourier transform infrared (FTIR) spectroscopy was performed on a Nicolet NEXUS 670 FTIR spectroscopy. The samples ((M)RSF) were dried completely and pressed with potassium bromide (KBr) using disks. The spectra were used to analyzing the change in the chemical structure of surface-treated fiber.

2.4.2. Tensile testing

The tensile test was done by using a tensile test machine (XL-100, Jilin Province Jinli Test Technology Co., Ltd.) adapted to the standard GB/T 1440-92. Specimens about 1 mm in thickness (as shown in Fig. 1) were cut from the plaques for the different measurements realized in the present study. The samples were placed for 48 h at room temperature (~25 °C) and atmospheric conditions (relative humidity of ~50 ± 5%) before test. The tensile rate was 1 mm/min.

2.4.3. Scanning electron microscopy

A field emission scanning electron microscope (FE-SEM, Hitachi High-Technologies CO.S-4300 model, Japan) was used to get SEM images of (M)RSF and PLA/(M)RSF composites. All specimens were fractured perpendicularly to the flow direction after immersion in liquid nitrogen for about 5 min. The fracture surface was sputter coated with gold to provide enhanced conductivity.

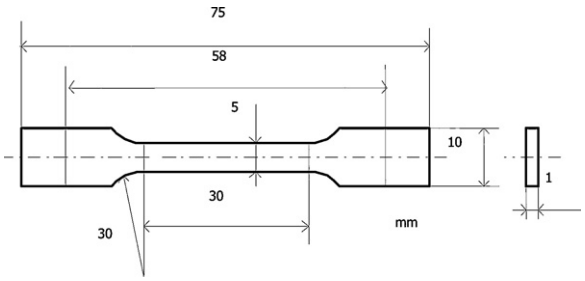

Fig. 1. Shape and measurement of specimens (mm).

2.4.4. Water absorption

Samples with dimensions 50 mm × 10 mm × 1 mm were cut from tensile specimens and used to examine the water absorption behavior after vacuum drying at room temperature for 24 h. The samples were immersed in distilled water (25 °C) for one week and taken out of water at each 24 h. The replicates were tested for each treatment. The percentage of water absorption (PWA) was calculated by the expression:

$$\mathrm{PWA} = \frac{W_f - W_i}{W_i} \times 100 \quad (3)$$

where W_f and W_i are the final and initial weights, respectively.

2.4.5. Thermogravimetric analysis

Thermogravimetric analysis (TGA) was performed on a TA Instrument 2050 TGA analyzer (Japan) recording the weight loss as a function of temperature. Samples were heated from 45 to 500 °C at a scanning rate of 10 °C/min in air. Degradation temperature values (T_d) were evaluated as temperatures corresponding to the maximum rate of the weight loss.

2.4.6. Differential scanning calorimetry

Thermal analysis of specimens was carried out using a sapphire DSC (Perkin-Elmer, America). The samples used for testing were sliced from the specimens. About 10 mg of dried samples were scanned at a heating rate of 10 °C/min under a 20 ml/min flow of nitrogen to prevent oxidation. The first scan was to remove all residual moisture and erase any thermal history from 20 to 180 °C. The T_g was obtained from the second scan from 20 to 250 °C.

3. Results and discussion

3.1. Preparation of MRSF

The percentage of weight of PBA reacted on RSF (W(%)), and yield of homopolymerization of PBA on RSF (Y(%)) were calculated according to Eqs. (1) and (2), which were similar to that reported by Liu and Su [27] and Kaewtatip and Tanrattanakul [28]. Table 1 represents different W(%) and Y(%) of samples polymerized in a water bath for 6 h at 75 °C. As shown in Table 1, when the weight ratio is under 100:100, both values increase with the content of BA monomer increasing, higher W(%) value shows higher Y(%) value. When the ratio by weight is over 100:100, Y(%) value increases slowly and is close to the balance. However, the amount of BA monomer shows significant effect on W(%), and the higher BA content offers the higher W(%). This may be because that more BA monomer offers more opportunity for adsorbing and coating polymerization. This agrees with the findings from the literature that low concentration of monomer leads to decrease the active sites on the growing chains and low polymerization yields. On the contrary, high concentration of monomer leads to more homopolymerization [28].

3.2. FTIR analysis

Several characteristic peaks representing chemical functional groups are detected in the FTIR spectra of RSF, MRSF, PBA, and BA, as shown in Fig. 2. The spectrum of RSF (Fig. 2(a)) shows a broad absorption band characteristic of the OH stretching, from 3600 to 3200 cm^{-1}. Moreover, the intense band at 1633 cm^{-1} is attributed to olefinic C=C stretching vibration while the bands at 1241 and 1161 cm^{-1} are the results of C–O stretching of the carbohydrate [21]. Compared with the spectrum of Fig. 2(a), a new band at 1734 cm^{-1} appears in the spectra of MRSF (Fig. 2(b) and (c)), showing that PBA was adsorbed and coated on RSF. However, the characteristic peak at 1732 cm^{-1} appeared in Fig. 2(b) is

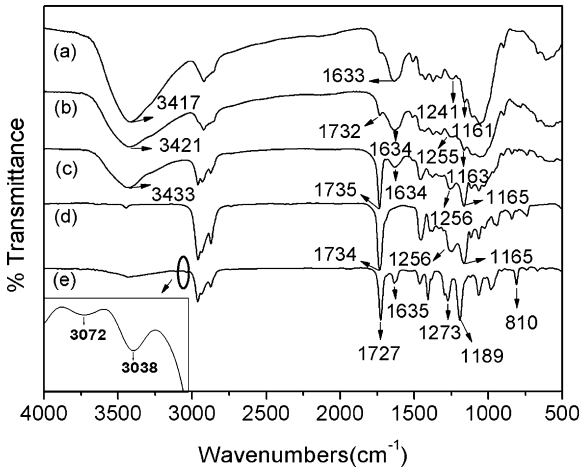

Fig. 2. FTIR spectrum of (a) RSF, (b) MRSF with W(%) = 7.98, (c) MRSF with W(%) = 132.9, (d) PBA, and (e) BA.

weak, which may be due to the little PBA content in the RSF [10]. This will be confirmed in the SEM images discussed in the subsequent section. The typical ester band appears in the PBA (Fig. 2(d)) at 1734 (C=O stretching), 1256 and 1165 cm^{-1} (C–O stretching) [27,29]. In the spectrum of BA, as shown in Fig. 2(e), the characteristic absorption bands at 3038 cm^{-1}, 3072 cm^{-1} and 1635 cm^{-1} can be attributed to C=C stretching vibration and the band at 810 cm^{-1} is the =CH out-of-plane bending modes [30]. However, the same absorption bands disappear in the spectrum of PBA (Fig. 2(d)). Moreover, it is not found C=C stretching vibration at 3038 cm^{-1}, 3072 cm^{-1} and =CH out-of-plane bending modes at 810 cm^{-1} in the spectra of MRSF (Fig. 2(b) and (c)). These results indicate that BA monomer has not been left in MRSF.

3.3. Morphology of the (M)RSF

SEM micrographs of RSF and MRSF (W(%) = 7.98, W(%) = 132.9) are shown in Fig. 3. The surface of RSF shows a very rough topography (Fig. 3(a)), while some sub-micron spherical particles of PBA and a continuous coating of PBA on RSF are observed in Fig. 3(b) and (c), respectively. The morphology suggests that the W(%) has great influence on their interior structure. The surface of MRSF with greater W(%) (Fig. 3(c)) remarkably shows the presence of PBA, compared with that of MRSF with smaller W(%) (Fig. 3(b)). This is corresponding with the foregoing FTIR results.

3.4. Tensile properties

According to Table 1, the specimen of PLA/(M)RSF composites are prepared with different W(%). The tensile strength of the composites was examined, as shown in Fig. 4. From Fig. 4, the tensile strength of PLA/RSF composites increases at first and then decreases with the increase of W(%), whereas the elongation at break increases slowly. Compared with S-1, the tensile strength of S-3 significantly increases by about 6 MPa which might be due to the little PBA coated and adsorbed on the RSF and good interfacial adhesion between MRSF and PLA matrix [31]. So we can conclude that little PBA may play an important role as a compatilizer. However, the tensile strength of PLA/MRSF decreases rapidly by further increasing the content of PBA. This may be due to the excess PBA (a very soft polymer) could not be dispersed well in the matrix and caused stress defects and induced the poor interfacial adhesion between PLA and MRSF, which reduced the strength.

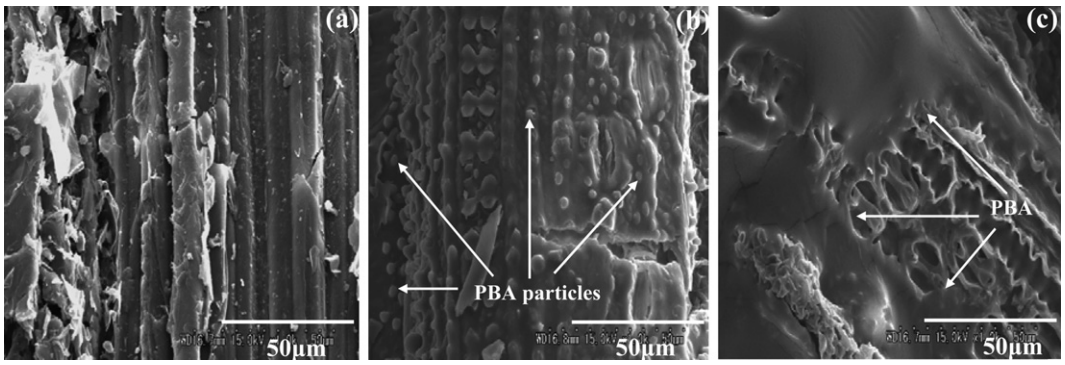

Fig. 3. SEM of (M)RSF (a) RSF, (b) MRSF with *W*(%) = 7.98, and (c) MRSF with *W*(%) = 132.9.

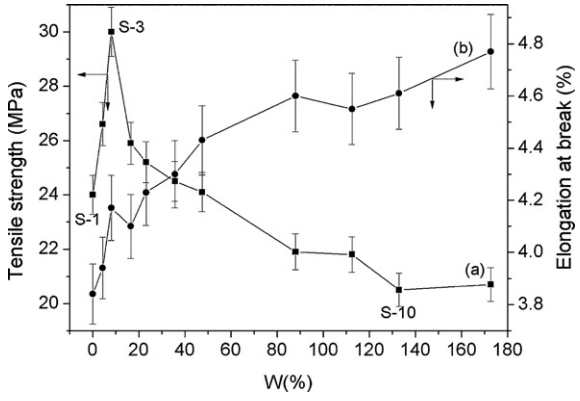

Fig. 4. Relationship between tensile property and additive rate of PBA: (a) tensile strength (MPa) and (b) elongation at break (%).

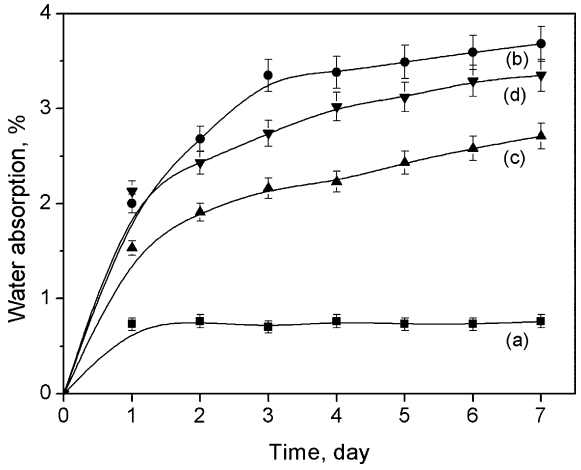

Fig. 6. Water absorption of PLA/(M)RSF composites: (a) PLA, (b) S-1, (c) S-3, and (d) S-10.

3.5. Morphology of the composites

The fracture surface morphology of PLA/(M)RSF composites was analyzed by SEM, as shown in Fig. 5. From Fig. 5(a), pullout of fiber from the matrix is observed, indicating poor adhesion between RSF and PLA [32,33]. Conversely, PLA/MRSF composite of S-3 (Fig. 5(b)) shows MRSF is broken off, which indicates good interfacial adhesion between the MRSF and PLA matrix. This effectiveness in the interfacial adhesion of the phases can be attributed to the different chemical structures and degree of functional groups affects the degree of interaction between the phases of the composites. PLA/MRSF composite of S-10 (Fig. 5(c)) has a different fracture surface compared with S-3 (Fig. 5(b)). Some of stacked PBA are shown in Fig. 5(c) which is due to the poor compatibility between PLA and MRSF when PBA content is high. These images indicate that excess PBA that cannot be dispersed well and stacked in the matrix and induced the poor interfacial adhesion. It was reported that the interfacial interaction affects the mechanical properties of the composite [31], which has been confirmed by the tensile test results discussed in the foregoing section. Therefore, the difference in fracture surface morphology of the PLA/MRSF composites may explain why the tensile strength of PLA/MRSF composite rapidly decreased when PBA content is over *W*(%) = 7.98.

3.6. Water absorption

The water absorption capacity of PLA and PLA/(M)RSF composites is shown in Fig. 6. As expected, PLA (Fig. 6(a)) shows the lowest water absorption because of its hydrophobicity. However, the PLA/(M)RSF composites absorbed more water than PLA. These results are in good accordance with the published data which

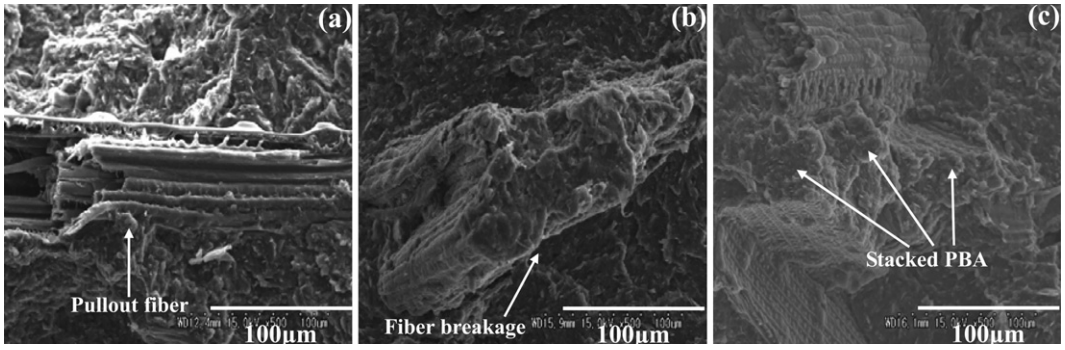

Fig. 5. SEM images of PLA/(M)RSF composites: (a) S-1, (b) S-3, and (c) S-10.

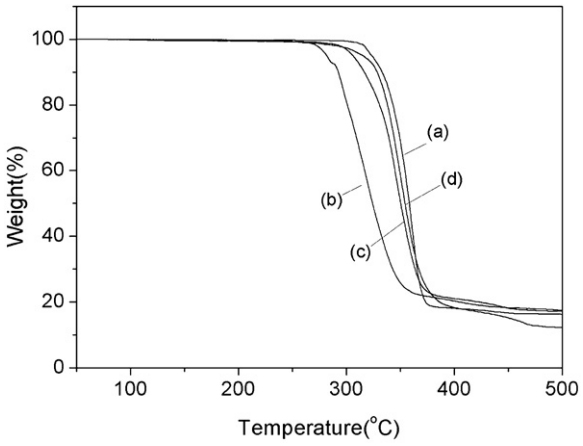

Fig. 7. TGA thermograms of PLA/(M)RSF composites: (a) PLA, (b) S-1, (c) S-3, and (d) S-10.

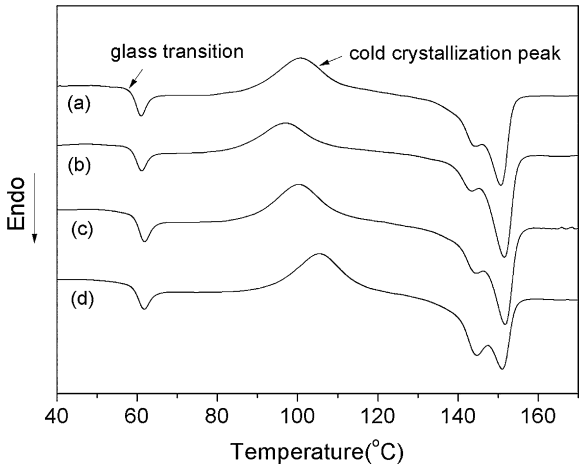

Fig. 8. DSC thermograms of samples: (a) PLA, (b) S-1, (c) S-3, and (d) S-10.

Table 2
Thermogravimetric data of the samples: degradation temperature (T_d) and residual weight at 500 °C.

Samples	T_d (°C)	Weight residual at 500 °C (%)
PLA	324	16.4
S-l	275	17.4
S-3	294	17.1
S-10	309	12.2

showed that the lignocellulosic polar fibers displayed a higher tendency to absorb water than the hydrophobic PLA [23]. Compared with the S-3 (Fig. 6(c)) and S-10 (Fig. 6(d)), S-1 (Fig. 6(b)) shows the highest water absorption. A possible reason for this behavior could be that PBA adsorbed and coated on RSF reduces the water absorbance capability of the composite, since PBA is a hydrophobic polymer [34]. However, the water absorption of S-10 is higher than S-3, which may be because that the S-3 has better interfacial adhesion that decrease the width of the interface area between the fibers and the composite decreases the water absorption through this area into inner parts of the material [35]. It was reported that a strong fiber/matrix interfacial adhesion can help to diminish the water penetration, reducing the hygroscopicity, and, consequently, avoiding the worsening of mechanical performances of composites [23]. This has been confirmed by the tensile test results and morphology of the composites.

3.7. TGA

The thermal degradation of PLA/(M)RSF composites has been investigated in terms of weight loss by TGA carried out in air as shown in Fig. 7. The residual weight is presented in graphical form as a function of temperature for PLA/(M)RSF composites. Table 2 shows the degradation temperature values (T_d) calculated as the maximum of degradation rate, and the residual weight at 500 °C. It can be observed that PLA/MRSF composites show higher thermal stability than PLA/RSF composites and a higher *W*% brings about higher thermal stability, degradation temperature values of S-1, S-3, S-10 composites are 275 °C, 294 °C and 309 °C, respectively. However, the presence of RSF decreases the T_d from 324 °C to 275 °C due to the nature of the RSF [13]. Concerning the residual weight at 500 °C, it can be remarked that S-10 composite shows a low residual weight, about 12%. PBA has very little ash after thermal degradation. So the major percentage of weight loss derives mainly from BA homopolymer [28]. As a consequence, the residual weight at 500 °C decreases with increasing *W*(%). This can explain why S-3 composites show a higher residual weight than S-10. The TGA results confirm the content of PBA increases in thermal stability of PLA/RSF composites.

3.8. DSC analysis

DSC experiment was carried out to investigate the thermal properties of the blend materials. Fig. 8 and Table 3 show the thermograms and numerically analyzed data of PLA and its composites, respectively. As can be seen in Fig. 8, an endothermic peak (in all the specimens) exists near the glass transition phase because of physical aging of the polymeric materials [36,37]. This phenomenon is related to the inherent distribution of the relaxation times of polymer chains. It can also be observed that cold crystallization peaks exist for the composite specimens. Interestingly, all melting endotherms show two distinct peaks, as show in Fig. 8. There may be two causes. Few authors have reported [38,39] this behavior as a result of lamellar rearrangement during crystallization of PLA: low-temperature peak is formed on the melting endotherm of the original crystallites, and the high-temperature peak is formed on the melting endotherm of the recrystal crystallites. In another case, the two melting peaks may be a result of the polymorphic crystalline transition of PLA [38]. In the present study,

Table 3
DSC analysis of the samples.

Samples	T_g (°C)	T_{cc} (°C)	ΔH_{cc} (J/g)	T_m (°C)		ΔH_m (J/g)	χ_c (%)
				T_{m1} (°C)	T_{m2} (°C)		
PLA	58.8	100.4	−17.0	144.1	150.6	27.0	10.7
S-l	58.8	96.7	−14.6	143.4	15L5	28.6	16.6
S-3	59.4	99.9	−16.3	144.1	151.7	24.5	9.80
S-10	59.1	105.3	−16.5	144.8	151.0	22.7	8.33

T_{cc}, cold crystallization temperature; ΔH_{cc}, cold crystallization enthalpy; T_{m1}, temperature of lower melting peak; T_{m2}, temperature of higher melting peak; T_g, glass transition temperature; ΔH_m, melting enthalpy; χ_c, degree of crystallinity.

the double-melting peak behavior observed in the PLA/(M)RSF composites when RSF was treated with PBA may be attributed to two different types of crystalline structures (e.g., variation in thickness of the lamellar structure and size of the spherulites) obtained during the crystallization process due to the influence of PBA [40].

The cold crystallization temperature (T_{cc}) decrease to 4 °C for S-1 compared with PLA. This agrees with the findings from the literature that the presence of fillers can promote the initial cold crystallization of PLA matrix [41]. However, the T_{cc} increases with the addition of PBA. This behavior indicates that PBA makes crystallization of PLA more difficult and incomplete. So when the content of PBA is high (W(%) = 132.9), PLA/MRSF composites have higher T_{cc} and poor crystallinity (χ_c).

The crystallinity (χ_c) of PLA is computed using Eq. (3) [42,43]:

$$\chi_c(\%) = \frac{\Delta H_m}{\Delta H_m^0} \times \frac{100}{w} \quad (4)$$

where w is the weight fraction of PLA in the sample, ΔH_m and ΔH_m^0 are the enthalpy for melting and that for a 100% crystalline PLA sample (93.7 J/g), respectively. To determine the crystallinity of the sample, the extra heat absorbed by the crystallites formed during heating (i.e., cold crystallization) have to be subtracted from the total endothermic heat flow due to the melting of the whole crystallites [44]. Thus, the modified equation can be written as follows:

$$\chi_c(\%) = \frac{\Delta H_m - \Delta H_{cc}}{\Delta H_m^0} \times \frac{100}{w} \quad (5)$$

where ΔH_{cc} is the enthalpy for cold-crystallization.

As can be inferred from Table 3, the addition of RSF enhances the crystallinity of PLA from 10.7% to 16.6% for S-1 sample. So, it can be concluded that the addition of RSF increases the crystallinity by acting as a nucleating agent. This agrees with the finding from the literature that the addition of fillers enhances the crystallinity of PLA [40,45,46]. However, the addition of PBA reduces the crystallinity of PLA, which indicates that PBA has played an important role in reducing the crystallinity of PLA/MRSF composites. This is because that PBA is situated at the surface of the fiber which inhibits the PLA from nucleating on the fiber. As stated earlier, PBA makes crystallization of PLA more difficult and incomplete. In addition, it can be seen that both T_g and T_m of the composites are not significantly different from the pure PLA.

4. Conclusion

Composites consisting of PLA and MRSF with PBA were prepared to improve the mechanical and thermal properties. The synthesis of MRSF was carried out from BA monomer and RSF by suspension polymerization. FTIR and SEM indicated that PBA was adsorbed and coated on RSF. The modified effect of the PBA on the mechanical and thermal properties has been investigated. A morphological study of PLA/MRSF (W(%) = 7.98) via SEM showed good interfacial adhesion between PLA and RSF and good dispersion of RSF in the polymer. However, the poor interfacial adhesion between PLA and RSF was observed when PBA content was high. These were well confirmed in the tensile test, which showed the tensile strength of PLA/RSF composites significantly increased to 6 MPa when W(%) = 7.98. But the tensile strength of PLA/RSF rapidly decreased while the content of PBA was over W(%) = 7.98. The addition of PBA to PLA led to decrease in tensile strength while the elongation at break was slowly increased. This is in good-agreement with the results of the water absorption test. TGA showed that the addition of PBA increased in thermal stability of PLA/RSF composites. DSC measurements deduced the following conclusions: the presence of PBA increased the cold crystallization temperature (T_{cc}) and reduced the crystallinity of PLA, the addition of RSF enhanced the crystallinity of PLA. However, both T_g and T_m of the composites were not significantly different from the pure PLA. In summary, PBA was not a good suitable potential compatilizer when the content of PBA was high. The optimum modification effect (W(%) = 7.98) was obtained where samples have good tensile strength and thermal stability.

References

[1] K. Sudesh, T. Lwata, Sustainability of biobased and biodegradable plastics, Clean 36 (2008) 433–442.
[2] M. Karin, E. Almgren, K. Gamstedt, F. Berthold, M. Lindström, Moisture uptake and hygroexpansion of wood fiber composite materials with polylactide and polypropylene matrix materials, Polym. Compos. 30 (2009) 1809–1816.
[3] A.K. Bledzki, J. Gassan, Composites reinforced with cellulose based fibres, Prog. Polym. Sci. 24 (1999) 221–274.
[4] D.N. Saheb, J.P. Jog, Natural fiber polymer composites—a review, Adv. Polym. Technol. 184 (1999) 351–363.
[5] D.K. Chen, J. Li, J. Ren, Study on sound absorption property of ramie fiber reinforced poly(L-lactic acid) composites: morphology and properties, Composites: Part A 41 (2010) 1012–1018.
[6] S.S. Wong, R. Shanks, A. Hodzic, Properties of poly(3-hydroxybutyric acid) composites with flax fibres modified by plasticiser absorption, Macromol. Mater. Eng. 287 (2002) 647–655.
[7] S. Pilla, S.Q. Gong, E. O'Neill, L.Q. Yang, R.M. Rowell, Polylactide-recycled wood fiber composites, J. Appl. Polym. Sci. 111 (2009) 37–47.
[8] M. Shibata, K. Ozawa, N. Teramoto, R. Yosomiya, H. Takeishi, Biocomposites made from short abaca fiber and biodegradable polyesters, Macromol. Mater. Eng. 288 (2003) 35–43.
[9] P.J. Pan, Y. Inoue, Polymorphism and isomorphism in biodegradable polyesters, Prog. Polym. Sci. 34 (2009) 605–640.
[10] M. Avella, G.B. Gaceva, A. Buzarovska, M.E. Errico, G. Gentile, A. Grozdanov, Poly(lactic acid)-based biocomposites reinforced with kenaf fibers, J. Appl. Polym. Sci. 108 (2008) 3542–3551.
[11] N.W. Zhang, Q.F. Wang, J. Ren, L. Wang, Preparation and properties of biodegradable poly(lactic acid)/poly(butylene adipate-co-terephthalate) blend with glycidyl methacrylate as reactive processing agent, J. Mater. Sci. 44 (2009) 250–256.
[12] R.E. Drumright, R.P. Gruber, E.D. Henton, Polylactic acid technology, Adv. Mater. 12 (2000) 1841–1846.
[13] K.H. Wang, T.M. Wu, Y.F. Shih, C.M. Huang, Water bamboo husk reinforced poly(lactic acid) green composites, Polym. Eng. Sci. 48 (2008) 1833–1839.
[14] T.M. Wu, C.Y. Wu, Biodegradable poly(lactic acid)/chitosan-modified montmorillonite nanocomposites: preparation and characterization, Polym. Degrad. Stab. 91 (2006) 2198–2204.
[15] S.M. Li, J. Ren, H. Yuan, T. Yu, W.Z. Yuan, Influence of ammonium polyphosphate on the flame retardancy and mechanical properties of ramie fiber-reinforced poly(lactic acid) biocomposites, Polym. Int. 59 (2010) 242–248.
[16] J. Ren, Q.F. Wang, S.Y. Gu, N.W. Zhang, T.B. Ren, Chain-linked lactic acid polymers by benzene diisocyanate, J. Appl. Polym. Sci. 99 (2006) 1045–1049.
[17] M. Garcı′a, I. Garmendia, J. Garcı′a, Influence of natural fiber type in eco-composites, J. Appl. Polym. Sci. 107 (2008) 2994–3004.
[18] R.A. Shanks, A. Hodzic, D. Ridderhof, Composites of poly(lactic acid) with flax fibers modified by interstitial polymerization, J. Appl. Polym. Sci. 99 (2006) 2305–2313.
[19] S.S. Wong, R.A. Shanks, A. Hodzic, Poly(L-lactic acid) composites with flax fibers modified by plasticizer absorption, Polym. Eng. Sci. 43 (2003) 1566–1575.
[20] K.G. Satyanarayana, G.G.C. Arizaga, F. Wypych, Biodegradable composites based on lignocellulosic fibers—an overview, Prog. Polym. Sci. 34 (2009) 982–1021.
[21] P. Fu, S. Hu, J. Xiang, L.S. Sun, T. Yang, A.C. Zhang, J.Y. Zhang, Mechanism study of rice straw pyrolysis by Fourier transform infrared technique, Chin. J. Chem. Eng. 17 (2009) 522–529.
[22] T. Murata, J.H. Qiu, M. Zhang, M.Z. Liu, L. Shang, M. Kudo, Y. Li, Mechanical Properties and Morphologies Observation of Biodegradable Polymer Composites Filled with Rice Straw, vol. 12, International Information Institute, 2009, pp. 1121–1126.
[23] T. Dobreva, R. Benavente, J.M. Pereña, E. Pérez, M. Avella, M. García, G. Bogoeva-Gaceva, Effect of different thermal treatments on the mechanical performance of poly(L-lactic acid) based eco-composites, J. Appl. Polym. Sci. 116 (2010) 1088–1098.
[24] J.X. Sun, F. Xu, Z.C. Geng, X.F. Sun, R.C. Sun, Comparative study of cellulose isolated by totally chlorine-free method from wood and cereal straw, J. Appl. Polym. Sci. 97 (2005) 322–335.
[25] B. Ndazi, J.V. Tesha, E.T.N. Bisanda, Some opportunities and challenges of producing bio-composites from non-wood residues, J. Mater. Sci. 41 (2006) 6984–6990.
[26] Y. Lemmouchi, M. Murariu, A.M.D. Santos, A. Amass, E. Schacht, P. Dubois, Plasticization of poly(lactide) with blends of tributyl citrate and low molecular weight poly(D,L-lactide)-b-poly(ethylene glycol) copolymers, Eur. Polym. J. 45 (2009) 2839–2848.
[27] P. Liu, Z.X. Su, Surface-initiated atom transfer radical polymerization (SI-ATRP) of n-butyl acrylate from starch granules, Carbohydr. Polym. 62 (2005) 159–163.

[28] K. Kaewtatip, V. Tanrattanakul, Preparation of cassava starch grafted with polystyrene by suspension polymerization, Carbohydr. Polym. 73 (2008) 647–655.
[29] J.S. Nunes, C.L. de Vasconcelos, T.N.C. Dantas, M.R. Pereira, J.L.C. Fonseca, Electrokinetic behavior of a poly(butyl acrylate-co methacrylic acid) latex, Colloids Surf. A 275 (2006) 148–152.
[30] S.J. Oh, S.C. Lee, S.Y. Park, Photopolymerization and photobleaching of n-butyl acrylate/fumed silica composites monitored by real time FTIR-ATR spectroscopy, Vib. Spectrosc. 42 (2006) 273–277.
[31] A.K. Saha, S. Das, D. Bhatta, B.C. Mitra, Study of jute fiber reinforced polyester composites by dynamic mechanical analysis, J. Appl. Polym. Sci. 71 (1999) 1505–1513.
[32] B.L. Shah, S.E. Selke, M.B. Walters, P.A. Heiden, Effects of wood flour and chitosan on mechanical, chemical, and thermal properties of polylactide, Polym. Compos. 29 (2008) 655–663.
[33] T. Yu, J. Ren, S.M. Li, H. Yuan, Y. Li, Effect of fiber surface-treatments on the properties of poly(lactic acid)/ramie composites, Composites: Part A 41 (2010) 499–505.
[34] J. Ren, Z.C. Liu, T.B. Ren, Mechanical and thermal properties of poly(lactic acid)/starch/montmorillonite biodegradable blends, Polym. Polym. Compos. 15 (2007) 633–638.
[35] P. Toro, R. Quijada, O. Murillo, M. Yazdani-Pedram, Study of the morphology and mechanical properties of polypropylene composites with silica or rice-husk, Polym. Int. 54 (2005) 730–734.
[36] I.M. Hodge, Effects of annealing and prior history on enthalpy relaxation in glassy polymers. 4. Comparison of five polymers, Macromolecules 16 (1983) 898–902.
[37] A.R. Berens, I.M. Hodge, Effects of annealing and prior history on enthalpy relaxation in glassy polymers. 1. Experimental study on poly(vinyl chloride), Macromolecules 15 (1982) 756–761.
[38] Z.J. Ren, L.S. Dong, Y.M. Yang, Dynamic mechanical and thermal properties of plasticized poly(lactic acid), J. Appl. Polym. Sci. 101 (2006) 1583–1590.
[39] Y. Wang, S.S. Funari, J.F. Mano, Influence of semicrystalline morphology on the glass transition of poly(L-lactic acid), Macromol. Chem. Phys. 207 (2006) 1262–1271.
[40] S. Pilla, S.Q. Gong, E. O'Neill, R.M. Rowell, A.M. Krzysik, Polylactide-pine wood flour composites, Polym. Eng. Sci. 48 (2008) 578–587.
[41] Z. Kulinski, E. Piorkowska, Crystallization, structure and properties of plasticized poly(L-lactide), Polymer 46 (2005) 10290–10300.
[42] R Vasanthakumari, A.J. Penning, Crystallization kinetics of poly(L-lactic acid), Polymer 24 (1983) 175–178.
[43] V.E. Reinsch, S.S. Kelley, Crystallization of poly(hydroxybutrate-co-hydroxyvalerate) in wood fiber-reinforced composites, J. Appl. Polym. Sci. 64 (1997) 1785–1796.
[44] J.Y. Nam, S.S. Ray, M. Okamoto, Crystallization behavior and morphology of biodegradable polylactide/layered silicate nanocomposite, Macromolecules 36 (2003) 7126–7131.
[45] R. Masirek, Z. Kulinski, D. Chionna, E. Piorkowska, M. Pracella, Composites of poly(L-lactide) with hemp fibers: morphology and thermal and mechanical properties, J. Appl. Polym. Sci. 105 (2007) 255–268.
[46] M. Pracella, D. Chionna, I. Anguillesi, Z. Kulinski, E. Piorkowska, Functionalization, compatibilization and properties of polypropylene composites with hemp fibres, Compos. Sci. Technol. 66 (2006) 2218–2230.